Journal of Physics: Conference Series **570** (2014) 072008 doi:10.1088/1742-6596/570/7/072008

Physically-based modeling of speed sensors for fault diagnosis and fault tolerant control in wind turbines

Wolfgang Weber[1], **Jonas Jungjohann**[2], **Horst Schulte**[2]

[1] Pepperl+Fuchs GmbH, 68307 Mannheim, Germany

[2] HTW Berlin, Department of Engineering I, Control Engineering, 12459 Berlin, Germany

E-mail: wweber@de.pepperl-fuchs.com, schulte@htw-berlin.de

Abstract.

In this paper, a generic physically-based modeling framework for encoder type speed sensors is derived. The consideration takes into account the nominal fault-free and two most relevant fault cases. The advantage of this approach is a reconstruction of the output waveforms in dependence of the internal physical parameter changes which enables a more accurate diagnosis and identification of faulty incremental encoders i.a. in wind turbines. The objectives are to describe the effect of the tilt and eccentric of the encoder disk on the digital output signals and the influence of the accuracy of the speed measurement in wind turbines. Simulation results show the applicability and effectiveness of the proposed approach.

1. Introduction

Due to the increasing dimensions and complexity of wind turbines, requirements regarding safety and availability continually rise. In particular, the increase of the equipment complexity caused an increase of probability of failure of individual components. Hence, in the recent years several approaches and methods have been proposed to detect and isolate faults in wind turbines on the system level which have been successfully applied in wind turbine simulation. A survey is given by the summary of a wind turbine FDI (fault detection and isolation) competition [1], where several actuator and sensor faults had to be detected within a pre-defined benchmark model [2]. In these studies, to prevent the loss of generality, a few sensor fault cases have been distinguished such as additive, scaling and fixed value faults. All of these are signal-based, which means the faults are modeled by event-triggered sensor signal adjustment in terms of signal addition, gain and compensation. Therefore the physical cause of faults in the sensor components are not previously considered. However, this information is useful to quantify the probability of occurrence and improved the fault reconstruction, both on the component and system level.

In this paper, a novel physically-based generic model of an incremental encoder, frequently used as rotor or generator speed sensor in wind turbines, is presented. In contrast to [2] a detailed mathematical model that takes into account the nominal case and systematic faults are proposed. Here, two relevant fault cases are studied in detail: First, the tilt of the encoder disk and second, the eccentric of the axis of rotation. The advantage of this approach is a reconstruction of waveforms in dependence of physical parameter changes which enables a more accurate fault identification.

This paper is organized as follows: In Section 2 the main components and control functions which have important influence on the performance of wind turbines, i.e. the energy production, are briefly described. Further, commonly used encoder types and their operating principles are presented. Sections 3 and 4 contain the main parts of this work. In Section 3 a generic white-box model framework for encoder type sensor systems is derived. The objective is to describe the effect of the tilt of the increment disk, the offset of the rotation axis on the digital output signals and the influence of the accuracy of the speed measurement. In Section 4, simulation studies including the nominal fault free and two common sensor fault cases are presented.

2. Sensors for wind turbine control

2.1. Functions of wind turbine control system

State of the art wind turbines in the 0.5 MW to 8 MW class have three major components which have important influence on the performance, i.e. the energy production of the system. First of all the nacelle including the rotor has to turn into the wind direction as good as possible. This function is called yaw and includes electrical drives which rotate the nacelle according to the signal of a wind measuring device (see Figure 2). The second function is called pitch and means the positioning of the rotor blades. Depending on the wind speed the rotor blade has to be adjusted in a way that a constant rotational speed is achieved (see Figure 1). Finally the rotor speed respectively the generator speed has to be determined (see Figure 3).
All these functions have performance as well as safety aspects. If the rotor speed exceeds a certain maximum value serious damage can happen, even the destruction of the wind turbine. Therefore, a safe shutdown function must be activated in case of exceeding the critical value. On the other hand the stand-still position of the rotor must be detected to enable safe access of service personnel.
If the nacelle turns with changing wind conditions there is a limit of revolutions into the same direction. A typical value is 3 to 4 turns into one direction. Exceeding this limit would cause the destruction of the cables which connect the power generation in the nacelle with the converters or other devices at the ground. Finally the determination of the blade position is crucial for the shutdown. Since up to date Mega Watt machines have rotors of huge size and weight like 20 tons or more, the full stop cannot be achieved by brakes any more. The rotor is controlled by turning the blades into a stall position to reduce the speed down to a value where the brakes could be safely applied.
Looking at all these functionalities it becomes obvious that a precise and reliable measuring of speeds and positions is a crucial aspect in the whole construction.

2.2. Encoder types for position and speed measurement

Traditionally there are two technical solutions to achieve this measuring task. In some cases inductive sensors are used to detect holes in a metal ring. By counting these incremental signals a control system could determine the actual speed but typically not a position. Therefore, incremental and absolute encoders have become state of the art, since they offer both types of signal and additionally a better resolution and precision. Because of the different requirements in the individual applications, there are a number of technologies and variants existing to provide solutions for each and every case:

- Incremental encoders with analogue or digital output (see Figure 4)
- Absolute encoders (single-turn; multi-turn)
- Absolute multi-turn encoders with
  - mechanical counter
  - battery buffered memory
- Absolute multi-turn encoders gearless, without battery by using Wiegand effect for counting

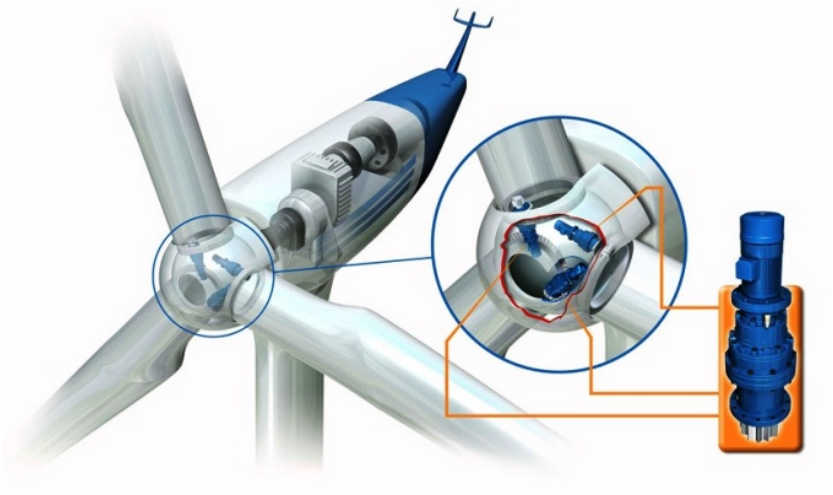

Figure 1. Shows the rotor of a wind turbine. The blade angle is adjusted according to the wind conditions to control the rotor speed.

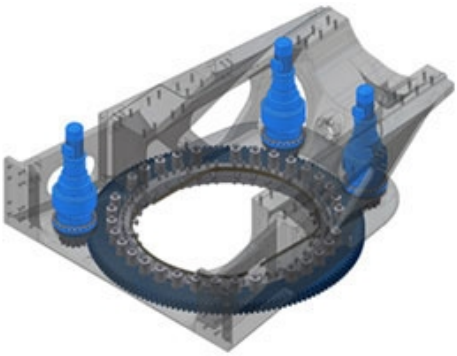

Figure 2. The nacelle is turned into the wind by electrical drives. The position of the nacelles must be determined and also the number of turns in either direction to prevent cable destruction.

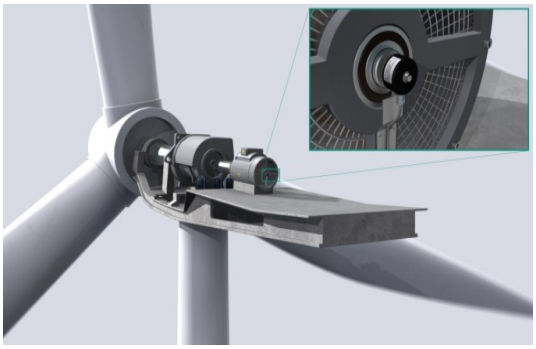

Figure 3. The rotor speed is measured directly at the low speed shaft and also at the fast moving generator shaft

- Absolute encoders with
  - fieldbus interfaces (CAN, Profibus, Profinet, EtherCAT, etc.)
  - magnetic, optical, capacitive or inductive working principle
  - non-contact magnetic or inductive encoder with external pole wheel.

Absolute encoders deliver position signals instead of incremental signals. The encoder disk contains a Gray Codes scale instead of simple one to one black and transparent transmissions. As an option absolute encoders can be executed as multi-turn versions, which keep counter values if the rotation exceeds 360 degrees several times. Nowadays optical systems are more and more replaced by magnetic encoders. The advantages of optical encoders were two-fold. Number one they could reach much higher rotational speed and number two they could deliver a much higher resolution. Newest developments have made at least the second point almost marginal. The resolution of magnetic encoders can reach up to 18 Bit, which lifts them to a

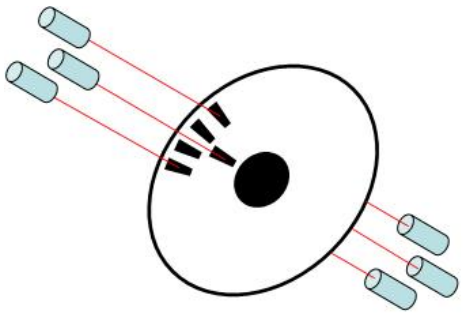

Figure 4. Typical arrangement of an incremental encoder. In case of an optical sensing system the encoder disk can be made of glass, plastic or metal. Two transmitter/receiver units detect the signal for the A and B signal. A third unit scans the zero position.

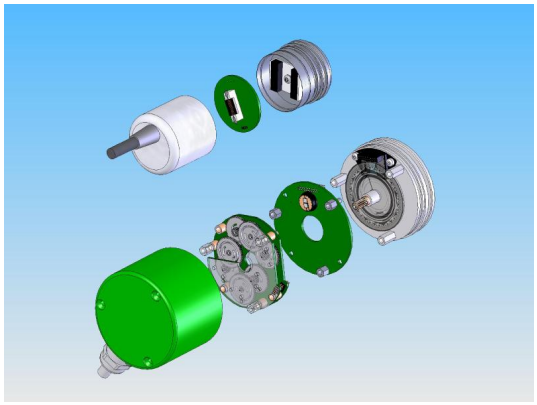

Figure 5. Comparison between two different encoder constructions. Both are multi-turn absolute encoders. One type shows an optical sensing system with a mechanical gear to count and store the multi-turn value. The other is a complete magnetic system with Wiegand wire for the multi-turn function.

comparable level as optical encoders. Since high revolutions do not take place in wind turbines but harsh environmental conditions became much more of an issue, magnetic encoders have become increasingly popular. The comparison in Figure 5 cearly shows that the magnetic version of a multi-turn encoder requires only a minimum of components and much less than the optical version with mechanical multi-turn unit. In addition to the increased robustness this has a significant influence on the life time calculation which shows in this specific case an advantage with a factor of 10.

Encoders are typically electro-mechanical devices (see Figure 6a). The mechanical parts are usually bearings. They are specifically subject to wear and tear. The calculation of the life-time of bearings is extremely difficult, because it depends heavily on external influences, such as temperature, kind of operation (low or high speed, long stand-still periods), type of grease or axial and radial axis loads. In most cases these environmental influences cannot clearly be specified. Therefore, there is a move in the direction of encoders without mechanical parts, respectively parts which are moving with mechanical contact.

In this case the magnet impulse unit is built in form of a ring which is placed outside the encoder detecting unit. This unit scans the magnetic field on a distance and is not touching anything (see Figure 6b). The detecting unit does not incorporate any moving mechanical parts, because it is sitting off-axis. One disadvantage of this construction is the small dimensional tolerance between the pole wheel and the sensor, which makes the installation in heavily vibrating machines impossible.

2.3. Accuracy of increments delivered by the output of an incremental encoder

There are various reasons why the signal of an incremental encoder is not 100% precise. In the state of the art products the electronic components are of sufficient quality and reliability. Usually limitations of the signal quality are caused by the mechanical construction. Especially manufacturing tolerances of different kind, such as eccentric or tilted mounting of the encoder disk or dimensional differences between the individual increments will cause limitations in the

Figure 6. A conventional encoder with ball bearings versus a non-contact magnetic encoder with pole wheel.

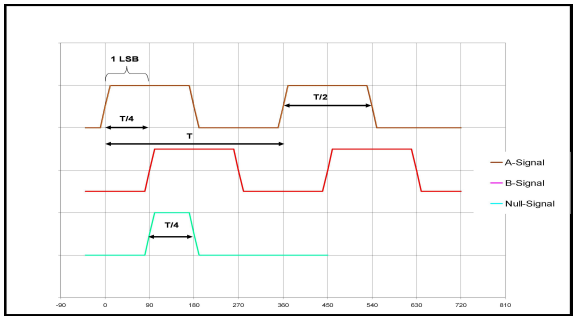

Figure 7. An encoder disk with 1024 increments and two channels (A + B) plus the zero track delivers 4 signal edges per increment. The $T/4$ measuring step is called the Least Significant Bit (LSB).

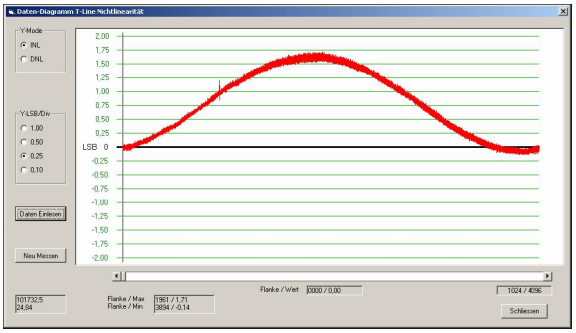

Figure 8. Measurement of the integral nonlinearity. The graph shows a maximum deviation of 1.71 LSB (see Figure 7)

achievable precision of the encoder signal.
There are two measurements which are typically executed to determine the accuracy of an incremental encoder. They are called differential and integral nonlinearity:

- The differential nonlinearity describes the dimensional deviation from each increment compared to the ideal model.
- The integral nonlinearity describes the summarized deviation over one revolution, which means the precision to reach exactly the same position after 360 degrees of rotation.

Taking the results shown in Figure 8 as an example the achievable accuracy would be 0.042%. Quiet often the encoder is coupled via a pinion wheel to the shaft or the drive. If such a pinion and the yaw bearing have a teeth ratio of 16 : 256 with a bearing diameter of 3 m, the positioning precision would be 0.063 m. If the same calculation would be applied on the revolution per minute of a rotor it would mean that at a typical value of 20 rpm the precision of the measurement would be 0.13 rpm.

3. Physically-based modeling of rotor/generator speed sensors

3.1. Model assumptions

As shown in Figure 4 an incremental encoder consists of light sources as transmitter, a receiver such as photodiodes or phototransistors, a rotating encoder disk and a stationary aperture. It is essential to mention that the modeling framework based on following assumptions:

(i) The aperture size A is taken as identical to the photosensitive surface of the sensor.

(ii) A pure ray optics is assumed. That is the light propagates in straight lines from the transmitter through the aperture to the receiver.

(iii) A homogeneous intensity distribution of the radiation causes a voltage signal that is propotional to the current aperture size A

$$u = \frac{A}{A_{max}} \tag{1}$$

with $u \in [0, 1]$ is a normalized voltage signal.

3.2. Nominal fault-free case

The current voltage signal or aperture size for a fixed axis results from the intersection of the aperture and encoder increment and can be determined by

$$A \;=\; \int_{\varphi=\varphi_1}^{\varphi=\varphi_2} \int_{r=r_i}^{r=r_a} r \; \mathrm{d}r \; \mathrm{d}\varphi \;=\; \frac{1}{2} \left(r_a^2 - r_i^2\right) \left(\varphi_2 - \varphi_1\right) \tag{2a}$$

where r_i and r_a are the constant radii of a encoder increment of one track (Figure 9), φ is the variable of integration and is limited by the circular arc of each increment with the bounds φ_1 and φ_2. Because the increment is not always completely over the aperture, the following cases have to be distinguished:

(i) Increasing sectional area

$$A \;=\; \int_{\varphi=\gamma_1}^{\varphi=\alpha_2} \int_{r=r_i}^{r=r_a} r \; \mathrm{d}r \; \mathrm{d}\varphi \tag{2b}$$

(ii) Constant sectional area

$$A \;=\; \int_{\varphi=\alpha_1}^{\varphi=\gamma_2} \int_{r=r_i}^{r=r_a} r \; \mathrm{d}r \; \mathrm{d}\varphi \tag{2c}$$

(iii) Decreasing sectional area

$$A \;=\; \int_{\varphi=\alpha_1}^{\varphi=\alpha_2} \int_{r=r_i}^{r=r_a} r \; \mathrm{d}r \; \mathrm{d}\varphi \tag{2d}$$

(iv) No sectional area

$$A \;=\; 0 \tag{2e}$$

where α_1, α_2 are the fixed aperture angles and γ_1, γ_2 are the angle of orifice area of one increment. For illustrating, the encoder geometry, all coordinates and variables are shown in Figure 9.

In the next step, we have to take into account the rotation of the encoder disk for the nominal case. For this purpose, without loss of generality, it is shortly and conveniently to consider a

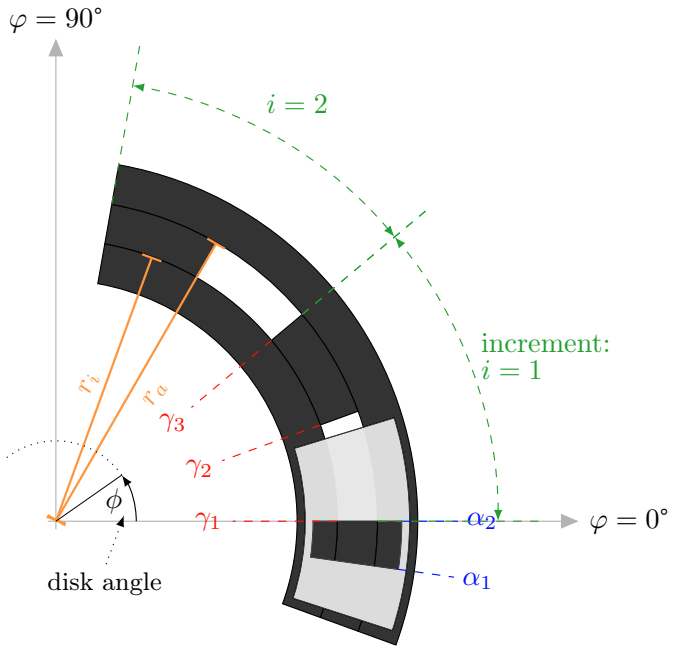

Figure 9. Geometry of aperture and increment disk for the fault-free case

rotating aperture instead of a rotating encoder disk. Using this approach, the aperture angle α_2 is equal to the current encoder disk angle ϕ. Therefore, the integral bounds can be determined by

$$\begin{aligned} \alpha_2 &= \phi \\ \alpha_1 &= \phi - \beta_B \ . \end{aligned} \tag{3}$$

where β_B is the orifice angle of the aperture. For the first increment this result to

$$\begin{aligned} \gamma_1 &= (i-1)\ \beta_I \\ \gamma_2 &= \gamma_1 + \beta_S \\ \gamma_3 &= \gamma_1 + \beta_I \end{aligned} \tag{4}$$

with β_S as angular width of increment orifice and β_I as angular width of increment $(2 \cdot \beta_S)$. The expression for γ_1 can be extended to $i \in \{2, 3, ...\}$ increments, see Figure 9. Further details can be found in [3]. Thus for each angular position the signal level is determined by previous equations (2) and (4).

3.3. Faulty case: Tilt encoder disk

Due to the manufacturing process the encoder disk can be tilt, so that disk and aperture are not parallel to each other. Then, the distance between disk and aperture is no longer constant and depends on the encoder disk angle ϕ. The tilt angle is denoted by ϑ and is related to the vertical disk position illustrated in Figure 10.

The starting point of the modeling approach is the parallel projection of an increment on the aperture plane. Instead of circles with constant radii r_i and r_a , a tilt encoder disk causes ellipse

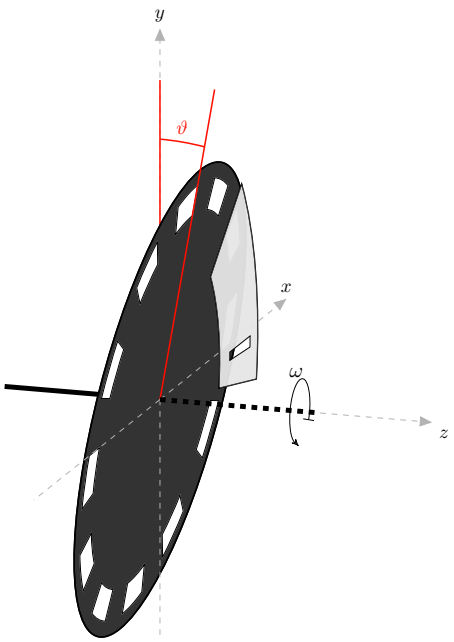

Figure 10. Tilt encoder disk

shaped projection of the increment edges on the aperture plane. This can be described by the following angle-dependent radii based on elliptic equation

$$r_i(\varphi) = \frac{r_{A_i} r_{B_i}}{\sqrt{(r_{A_i} \sin\varphi)^2 + (r_{B_i} \cos\varphi)^2}}, \quad r_a(\varphi) = \frac{r_{A_a} r_{B_a}}{\sqrt{(r_{A_a} \sin\varphi)^2 + (r_{B_a} \cos\varphi)^2}}$$

with

$$\begin{aligned} r_{A_i} &= r_i\,, & r_{B_i} &= r_i \cos\vartheta\,, \\ r_{A_a} &= r_a\,, & r_{B_a} &= r_a \cos\vartheta \end{aligned} \tag{5}$$

where r_A is the minor and r_B is the main axis of the ellipse. Taking this into account we get the integral representation to calculate the aperture size

$$A = \int_{\varphi=\varphi_1}^{\varphi=\varphi_2} \int_{r=r_i(\varphi)}^{r=r_a(\varphi)} r \,\mathrm{d}r\,\mathrm{d}\varphi = \int_{\varphi=\varphi_1}^{\varphi=\varphi_2} \frac{1}{2} r^2 \Big|_{r_i(\varphi)}^{r_a(\varphi)} \mathrm{d}\varphi = \frac{1}{2} \int_{\varphi=\varphi_1}^{\varphi=\varphi_2} r_a^2(\varphi) - r_i^2(\varphi)\,\mathrm{d}\varphi\,.$$

After analytical calculation of this integral we obtain the aperture size as a function of ϑ

$$A(\vartheta) = \frac{1}{2}\left(\arctan\left(\frac{1}{\cos\vartheta}\tan(\varphi_2)\right) - \arctan\left(\frac{1}{\cos\vartheta}\tan(\varphi_1)\right)\right)\left({r_a}^2\cos(\vartheta) - {r_i}^2\cos(\vartheta)\right)\,. \tag{6}$$

3.4. Faulty case: Eccentric axis of rotation

Due to manufacturing inaccuracy or age-related wear, it may be occur that the rotation axis is not exactly in the center of the increment disk. Then, similarly as in the previous case, r_i and r_a are not constant, and depending on the angle ϕ. In the following, it is assumed that

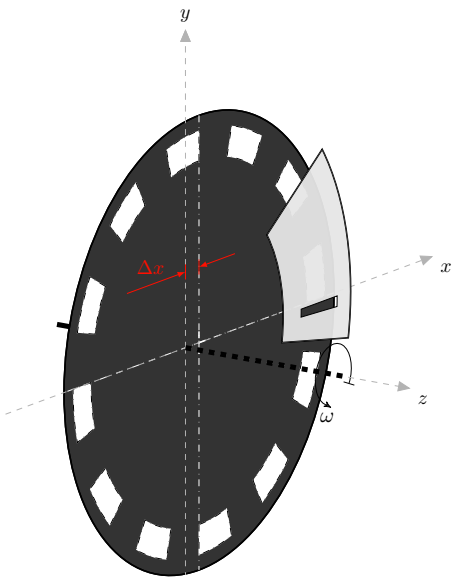

Figure 11. Eccentric axis of rotation

the displacement of the rotation axis can be described by Δx (see Figure 11) and the angle-dependent radii are denoted by $\tilde{r}_i$ and $\tilde{r}_a$. Applying the law of cosines to calculate $\tilde{r}_i$ and $\tilde{r}_a$, we get

$$\begin{aligned} {r_i}^2 &= \tilde{r}_i^2(\varphi) + \Delta x^2 - 2\,\tilde{r}_i(\varphi)\,\Delta x\,\cos(\varphi)\,, \\ {r_a}^2 &= \tilde{r}_a^2(\varphi)^2 + \Delta x^2 - 2\,\tilde{r}_a(\varphi)\,\Delta x\,\cos(\varphi)\,, \end{aligned}$$

and changed to the interesting quantities

$$\begin{aligned} \tilde{r}_i(\varphi) &= \Delta x\,\cos(\varphi) + \sqrt{{r_i}^2 - (\Delta x\,\sin(\varphi))^2}\,, \\ \tilde{r}_a(\varphi) &= \Delta x\,\cos(\varphi) + \sqrt{{r_a}^2 - (\Delta x\,\sin(\varphi))^2}\,. \end{aligned} \tag{7}$$

As for the previous case, the aperture size is

$$A = \int_{\varphi=\varphi_1}^{\varphi=\varphi_2} \int_{r=\tilde{r}_i(\varphi)}^{r=\tilde{r}_a(\varphi)} r\,\mathrm{d}r\,\mathrm{d}\varphi = \frac{1}{2} \int_{\varphi=\varphi_1}^{\varphi=\varphi_2} \tilde{r}_a^2(\varphi) - \tilde{r}_i^2(\varphi)\,\mathrm{d}\varphi \tag{8}$$

After substituting (7) in (8) and some calculation we get the aperture size as a function of the displacement of the rotation axis

$$
\begin{aligned}
A(\Delta x) \;=\; & \frac{1}{2}\left(\Delta x^2 \sin(\varphi_2)\left(\sqrt{\left(\frac{{r_a}^2}{\Delta x^2}-\frac{1}{2}\sin^2(\varphi_2)\right)}+\sqrt{\left(\frac{{r_i}^2}{\Delta x^2}-\frac{1}{2}\sin^2(\varphi_2)\right)}\right)\right. \\
& - \quad \Delta x^2 \sin(\varphi_1)\left(\sqrt{\left(\frac{{r_a}^2}{\Delta x^2}-\frac{1}{2}\sin^2(\varphi_1)\right)}+\sqrt{\left(\frac{{r_i}^2}{\Delta x^2}-\frac{1}{2}\sin^2(\varphi_1)\right)}\right) \\
& + {r_a}^2\left[\arctan\left(\frac{\Delta x\ \sin(\varphi_2)}{\sqrt{{r_a}^2\ 2\Delta x^2\sin^2(\varphi_2)}}\right)-\arctan\left(\frac{\Delta x\cdot\sin(\varphi_1)}{\sqrt{{r_a}^2\ 2\Delta x^2\sin^2(\varphi_1)}}\right)\right] \\
& - {r_i}^2\left[\arctan\left(\frac{\Delta x\ \sin(\varphi_2)}{\sqrt{{r_i}^2\cdot 2\Delta x^2\sin^2(\varphi_2)}}\right)-\arctan\left(\frac{\Delta x\ \sin(\varphi_1)}{\sqrt{{r_i}^2\ 2\Delta x^2\sin^2(\varphi_1)}}\right)\right] \\
& \left. + \ (\varphi_2-\varphi_1)\ ({r_a}^2-{r_i}^2)\right). \qquad (9)
\end{aligned}
$$

4. Impact of sensor faults on measurement accuracy

4.1. Signal processing

Finally, the impact of the fault cases on the sensor measurement accuracy are considered. First, the signal processing methods must be explained: In the first signal processing step, the raw analog signal A is transformed into a digital one by a comparator circuit. This digital signal is denoted by A_d. In order to ensure a high accuracy, sensor manufacturers use different circuit solutions for the same problem, which will not be discussed here. Then, in the second step, the current speed value n is calculated from the digital signal A_d. Two methods are commonly used:

(i) Counting the signal edges during a constant gate time T_g.

(ii) Measuring the time t_A that elapses between two successive signal edges.

The first method can be described by the expression

$$n = \frac{N_s}{T_g\ N} \qquad (10)$$

with n as the speed value, N as the number of increments on the encoder disk and N_s as the number of counted signal edges during the constant gate time T_g. The second method is given by

$$n = \frac{1}{t_A\ N} \qquad (11)$$

where t_A is the elapses time between two successive signal edges.

4.2. Impact of tilt encoder disk on measurement accuracy

The effects of a twisted encoder disk are illustrated by an example using a reasonable tilt angle $\vartheta = 0.75°$. For realistic results the two common methods for speed calculation (10) and (11) are taken into consideration. The speed variation over a sensor revolution with $N = 1024$ using (10) where $T_g = 10\,\text{ms}$ is shown in Figure 12. For comparison, the same faulty case is considered with the second signal processing method (11) (see Figure 13). With both methods

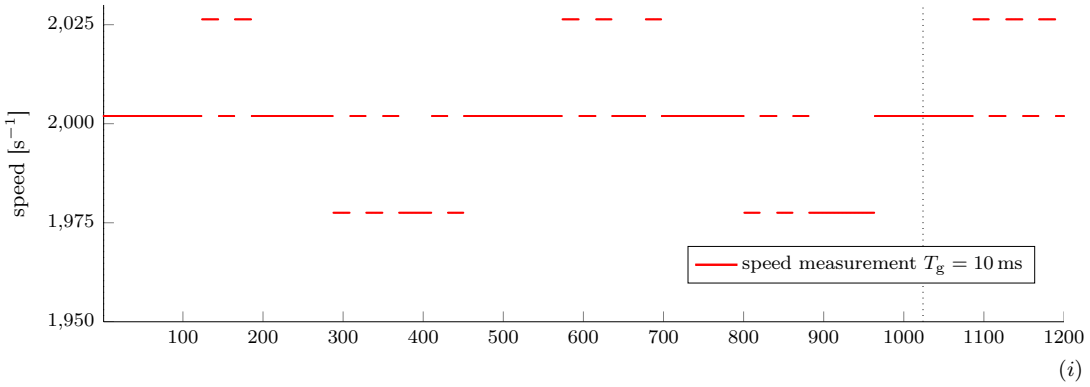

Figure 12. Effect on measured speed curve caused by a tilt encoder disk $\vartheta = 0.75°$ at true speed $n_0 = 2.0\,\text{s}^{-1}$ using (10) where $T_g = 10\,\text{ms}$ and $N = 1024$

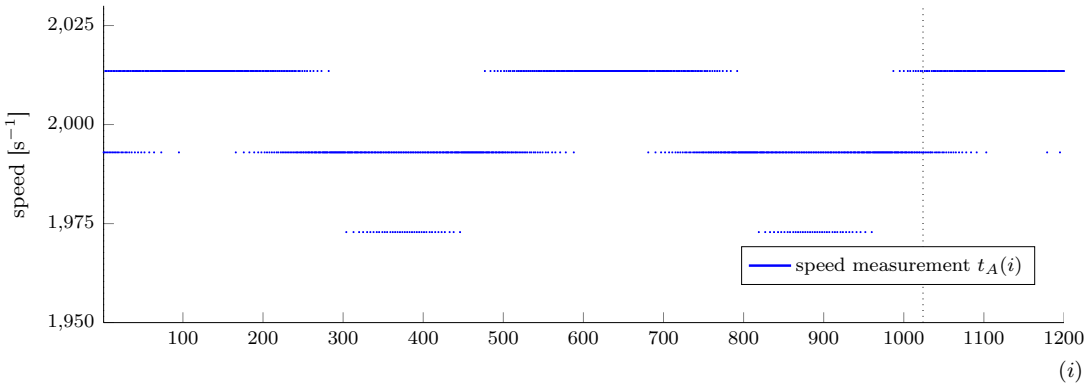

Figure 13. Effect on measured speed curve caused by a tilt encoder disk $\vartheta = 0.75°$ at true speed $n_0 = 2.0\,\text{s}^{-1}$ using (11) where $N = 1024$

it is clearly illustrated, that the simulated measured curves vary significantly about the true value $n_0 = 2.0\,\text{s}^{-1}$. The influence of the calculation methods are also clearly visible. Further simulations have shown, that the peak-to-peak value of n-curve increases with increasing tilt angle. But a purely analytical description of this relationship has not been derived yet.

4.3. Impact of eccentric rotation axis on measurement accuracy
Furthermore, the effects of a eccentric rotation axis are illustrated by a displacement of $\Delta x = 0.1\,\text{mm}$. As before, the two different methods for speed calculation are taken into consideration. The variation of the measured speed curve caused by displacement of the rotation axis calculated with (10) is shown in Figure 14. For comparison, the same fault is considerd with the second signal processing method (11). The simulation result is shown in Figure 15. Also in this case, it is illustrated that the simulated measured curves vary significantly about the true value $n_0 = 2.0\,\text{s}^{-1}$ influenced by a displacement of the rotation axis.

5. Conclusion and current work
In this paper, a generic physically-based model for encoder type speed sensors with an optical system was presented. Using the classical beam optics, the effect of tilt and eccentric of the

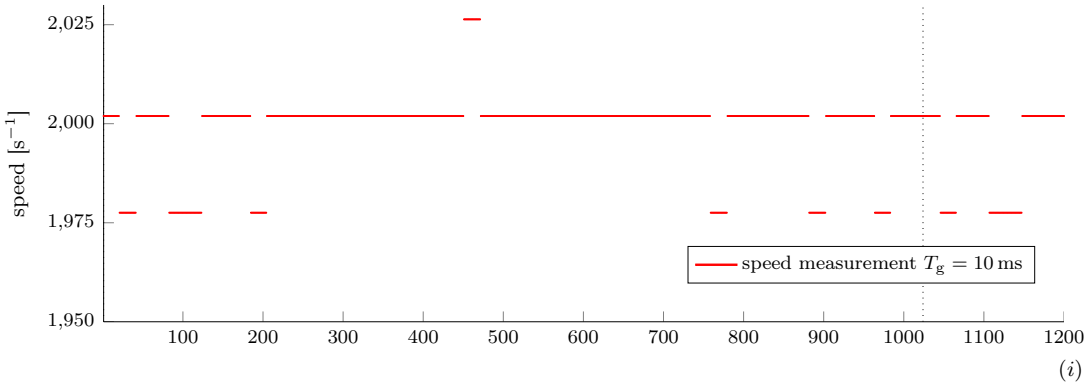

Figure 14. Effect on measured speed curve caused by displacement of the rotation axis $\Delta x = 0.1\,\text{mm}$ at true speed $n_0 = 2.0\,\text{s}^{-1}$ using (10) where $T_g = 10\,\text{ms}$ and $N = 1024$

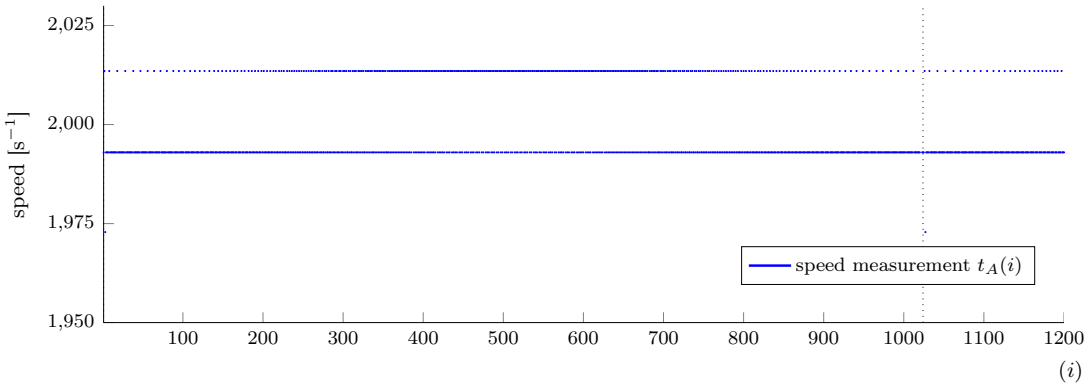

Figure 15. Effect on measured speed curve caused by displacement of the rotation axis $\Delta x = 0.1\,\text{mm}$ at true speed $n_0 = 2.0\,\text{s}^{-1}$ using (11) where $N = 1024$

encoder disk were analytically described as a function of the tilt angle and the displacement of the encoder axis. The influence of different methods of speed calculation was also investigated. On the basis of simulation studies using the analytical model the effects of non-nominal parameter values on the sensor speed signal could be made clearly visible. In current work, reduced models are derived with the objective to integrate these into the benchmark models [2] and [4] (based on [5],[6]) for a more realistic sensor failure scenarios for fault diagnosis of wind turbines.

References

[1] Odgaard P F and Stoustrup J 2012 *IFAC Symposium on Fault Detection, Supervision and Safety of Technical Processes* (Mexico City, Mexico) pp 102–107
[2] Odgaard P F, Stoustrup J and Kinnaert M 2009 *IFAC Symposium on Fault Detection, Supervision and Safety of Technical Processes* (Barcelona, Spain) pp 155–160
[3] Jungjohann J 2014 *Model-based fault identification for incremental encoders in wind turbines (in german)* Master Thesis, HTW Berlin, Control Engineering Group, (Berlin, Germany)
[4] Odgaard P F and Johnson K E 2013 *American Control Conference* (Washington D.C., USA), pp 4447–4452
[5] Jonkman, J (2010) NWTC Design Codes, FAST *http://wind.nrel.gov/designcodes/simulators/fast/* accessed 05-November-2010 (Colorado, USA)
[6] Jonkman, J, Butterfield S, Musial W, and Scott G (2009) *Definition of a 5-MW Reference Wind Turbine for Offshore Systems Development* NREL/TP-500-38060, Tech. Rep. (Colorado, USA)